Optics Letters

Broadband frequency comb generation through cascaded quadratic nonlinearity in thin-film lithium niobate microresonators

Chao Tang,[1,2,†] Mingming Nie,[3,4,†] Jia-Yang Chen,[1,2,†] Zhaohui Ma,[1,2] Zhan Li,[1,2] Yijun Xie,[3] Yong Meng Sua,[1,2] Shu-Wei Huang,[3,5] and Yu-Ping Huang[1,2,*]

[1]Department of Physics, Stevens Institute of Technology, 1 Castle Point Terrace, Hoboken, New Jersey 07030, USA
[2]Center for Quantum Science and Engineering, Stevens Institute of Technology, 1 Castle Point Terrace, Hoboken, New Jersey 07030, USA
[3]Department of Electrical, Computer & Energy Engineering, University of Colorado Boulder, Boulder, Colorado 80309, USA
[4]Mingming.Nie@colorado.edu
[5]ShuWei.Huang@colorado.edu
[†]These authors contributed equally to this Letter.
[*]yuping.huang@stevens.edu

Received 14 March 2024; revised 4 April 2024; accepted 4 April 2024; posted 9 April 2024; published 29 April 2024

Broadband frequency comb generation through cascaded quadratic nonlinearity remains experimentally untapped in free-space cavities with bulk $\chi^{(2)}$ materials mainly due to the high threshold power and restricted ability of dispersion engineering. Thin-film lithium niobate (LN) is a good platform for nonlinear optics due to the tight mode confinement in a nano-dimensional waveguide, the ease of dispersion engineering, large quadratic nonlinearities, and flexible phase matching via periodic poling. Here we demonstrate broadband frequency comb generation through dispersion engineering in a thin-film LN microresonator. Bandwidths of 150 nm (80 nm) and 25 nm (12 nm) for center wavelengths at 1560 and 780 nm are achieved, respectively, in a cavity-enhanced second-harmonic generation (doubly resonant optical parametric oscillator). Our demonstration paves the way for pure quadratic soliton generation, which is a great complement to dissipative Kerr soliton frequency combs for extended interesting nonlinear applications.

https://doi.org/10.1364/OL.523920

Introduction. Dissipative Kerr soliton (DKS) optical frequency combs (OFCs)—also known as "microcombs"—are sets of equidistant spectral lines generated via pumping a high-Q $\chi^{(3)}$ microresonator [1]. They have arguably created a new field in cavity nonlinear photonics, with a strong cross-fertilization among theoretical, experimental, and technological research. Notably, a delicate balance between parametric gain, cavity loss, the Kerr nonlinearity, and group velocity dispersion (GVD) enables versatile DKS frequency comb generation for a plethora of applications covering time–frequency metrology, spectroscopy, quantum sensing, microwave photonics, ultrahigh capacity optical fiber communication, and so on [1–3]. It has become a powerful OFC technology to realize the long-sought-after goal of a field-deployable precision metrology device in challenged remote and mobile environments.

Recently, there are growing interests to apply the principles of DKS frequency comb to $\chi^{(2)}$ microresonators [4–12] to substantially enhance the DKS frequency comb performances, such as ultralow DKS threshold power, DKS wavelength extension to visible and mid-infrared regime, self-starting operation, and broadband bi-chromatic DKS generation for on-chip f-2f self-referencing. In theory, frequency comb generation by pumping $\chi^{(2)}$ microresonators originates from the cascaded quadratic nonlinear processes, which leads to a much larger effective $\chi^{(3)}$ nonlinearity than the material-based $\chi^{(3)}$ nonlinearity [7,8,12]. However, group velocity mismatch (GVM) between the two interacting wavelengths limits the bandwidth of the effective $\chi^{(3)}$ nonlinearity and divides the quadratic comb generation into two regimes: a large walk-off regime and a small walk-off regime [7,8]. In an experiment, large walk-off-induced narrowband modulation instability and quadratic comb generation have been realized in either free-space cavities with a bulk periodic-poled lithium niobate (PPLN) crystal or monolithic PPLN crystal microresonators [4,5]. However, the demonstration of a broadband quadratic comb and soliton generation with a small walk-off is challenging, if not impossible, and remains rare especially in experiments.

Recent years have seen the prosperity of advanced power-saving micro-devices based on thin-film lithium niobate, such as electro-optic and acousto-optic modulators [13,14]. Moreover, a thin-film lithium niobate is a good platform for nonlinear optics due to the tight mode confinement in a nanowaveguide, strong ability of dispersion engineering [15], large quadratic nonlinear coefficient [16–18], and flexible phase matching via optical domain inversion.

In this Letter, we demonstrate broadband frequency comb generation with a small walk-off through cascaded quadratic nonlinearity in thin-film lithium niobate microresonators. First, we design and fabricate a PPLN microresonator with a near-zero group velocity mismatch (GVM) of 52 fs/mm through dedicated dispersion engineering. Then, by pumping the microresonator at 1560 nm, the normalized efficiency of the second-harmonic

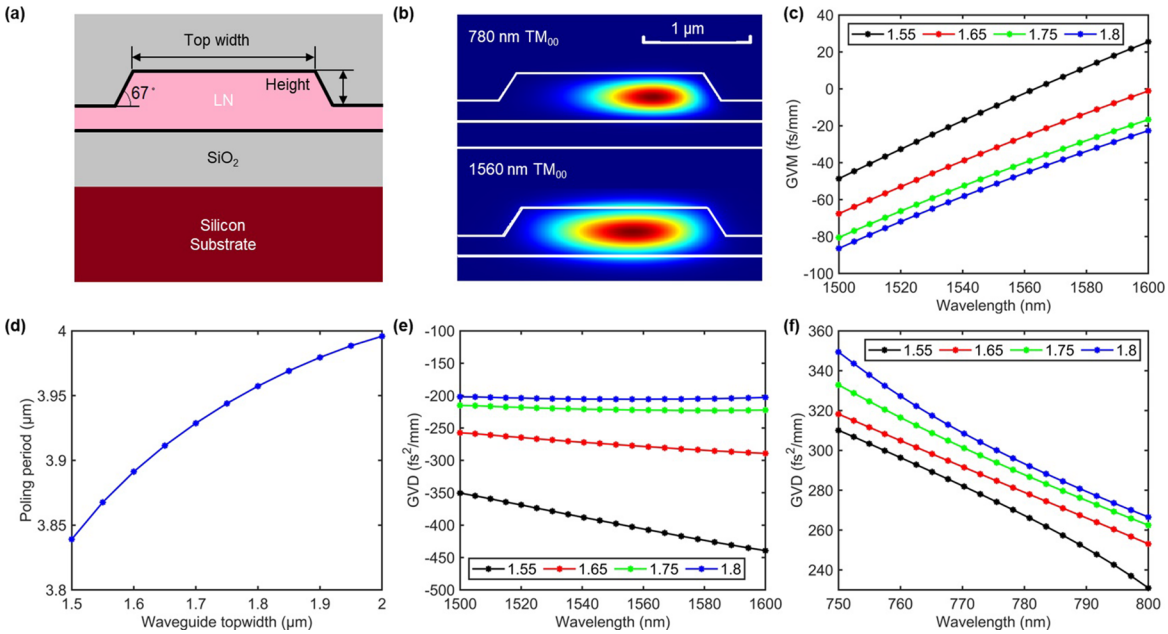

Fig. 1. Microresonator design. (a) Waveguide dimension; (b) mode profiles; (c) wavelength-dependent GVM with different top widths; (d) top-width-dependent poling period at 1560 nm; (e) wavelength-dependent GVD with different top widths at the near-infrared band; (f) wavelength-dependent GVD with different top widths at the visible band.

generation (SHG) in the cavity-enhanced doubly resonant system reaches normalized efficiency of 137,000%/W before comb generation. Finally, bandwidths of 150 nm (80 nm) and 25 nm (12 nm) for center wavelengths at 1560 and 780 nm are achieved, respectively, in a cavity-enhanced second-harmonic generation (doubly resonant optical parametric oscillator), which agree well with the simulation results. Our demonstration paves the way for pure quadratic soliton generation, which is a nice complement to dissipative Kerr soliton frequency combs with higher energy efficiency and for more interesting nonlinear applications.

Microresonator design and characterization. According to our previous theoretical analysis [3], a low GVM between the two bands is required to achieve broadband cascaded second-order nonlinearity. A z-cut PPLN microresonator using a type-0 phase matching condition (all fundamental transverse-magnetic modes: $TM_{00} + TM_{00} \rightarrow TM_{00}$) could allow zero GVM between 1560 and 780 nm. Figures 1(a) and 1(b) show the typical dimension and mode profiles of the designed microresonators with a radius of 80 μm and total thickness of 700 nm [19]. The etched height is set to be 410 nm, the top width is set to be 1.8 μm, and the base angle is set to be 67°. The designed poling period is 3.96 μm. To find the perfect group-velocity-matched geometry, in the simulation the microresonator top width is scanned from 1.55 to 1.8 μm while other parameters are kept unchanged. As shown in Fig. 1(c), in theory a top width of 1.55 μm gives a perfectly zero GVM. However, due to the inevitable fabrication errors, the uneven thickness of the wafer [20], and the waveguide geometry-dependent poling period (see Fig. 1(d)), in the experiment, it is difficult to simultaneously obtain the designed dispersion relationships as well as the phase matching condition. As the top width error is the main error origin during the fabrication process, the top width is changed with a step size of 50 nm as well as the poling period with a step size of 50 nm to find a zero GVM, phase-matched PPLN microresonator within the Er-doped fiber amplifier (EDFA) spectral band. In Figs. 1(e) and 1(f), we plot the wavelength-dependent group velocity dispersion (GVD) with different top widths. As seen, the GVDs for the two bands are of opposite signs: anomalous dispersion for the near-infrared band and normal dispersion for the visible band.

Figure 2(a) shows the scanning electron microscopy (SEM) images of one of the fabricated PPLN microresonators. Figure 2(b) shows the experimental setup for microresonator characterization and comb generation. To measure the quality (Q) factor in both wavelength bands, frequency-calibrated tunable lasers at 1560 nm (Santec TSL-550) and 780 nm are used, where the latter is obtained from the SHG of the same amplified 1560-nm tunable laser in a bulk PPLN crystal. Both near-IR and visible lasers are coupled into the chip using a lensed fiber by first combining them with a 780 nm/1560 nm wavelength division multiplexer (WDM).

In the experiment, we first test the phase matching condition at different temperatures by scanning the frequency of the continuous-wave (CW) pump laser with a low pump power and simultaneously monitoring the second-harmonic output, which will be discussed later in detail. The chosen microresonator has a top width of 1.8 μm since it is expected to provide the best phase matching in the C and L band regimes. As shown in Figs. 2(c) and 2(d), the loaded (coupled, intrinsic) Q factors Q_L (Q_C, Q_0) at 1560 and 780 nm are measured to be 1.5 (2.1, 5.0) $\times 10^5$ and 0.6 (0.67, 5.6) $\times 10^5$, respectively, when measured with a low on-chip power (~50 μW). Of note, the microresonator is over coupled for high conversion efficiency from pump to combs. The simultaneous frequency scanning process in Fig. 2(b) also helps quantify the offset frequency between the two resonances for both wavelengths in the time domain, assuming the linear frequency scanning. This is advantageous to find the precise pump wavelength to match the doubly resonant and phase matching condition.

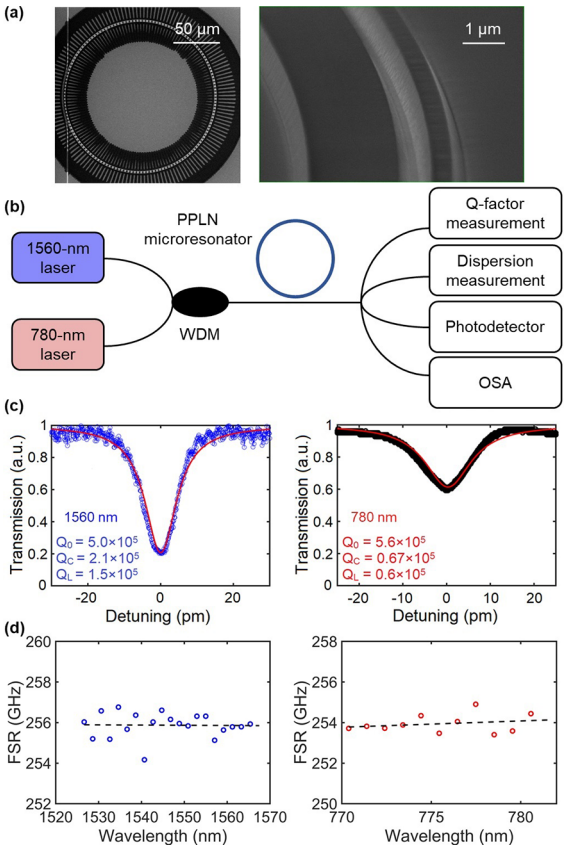

Fig. 2. Microresonator characterization. (a) SEM images of the periodically poled LN microresonator; (b) experimental setup; (c) measured Q factors for 1560 and 780 nm; (d) wavelength-dependent FSR for 1560 and 780 nm. a.u., arbitrary units.

As for the dispersion measurement, a frequency-calibrated Mach–Zehnder interferometer (MZI) with a free spectral range (FSR) of ~1 MHz is employed to precisely measure the GVM and GVD [21,22]. According to the measured wavelength-dependent FSRs in Figs. 1(d) and 1(e), the calculated GVM at 1560 nm is 52 fs/mm, as $1/(FSR_1{*}L) - 1/(FSR_2{*}L)$, with FSR_1 and FSR_2 the free spectral ranges of 1560 and 780 nm, and L the round trip length. The result agrees well with the simulated result in Fig. 1(c). The GVDs for both wavelengths are calculated to be −32 and 553 fs^2/mm. The mismatch between the simulation and experiment can be attributed to fabrication errors, wafer defects, and the avoided mode crossings [23].

SHG at a low input power. In Fig. 3(a), we measure the bandwidth of the SHG by scanning the pump frequency. Assuming both resonances are well aligned and perfectly phase-matched at 1560 and 780 nm, a small GVM-induced small FSR difference can enable the phase matching over a large bandwidth. Therefore, the bandwidth of the SHG can be an indicator of GVM. The SHG bandwidth of ~40 nm implies a GVM of ~111 fs/mm, which agrees with our measured results of 52 fs/mm in Fig. 2(d). We also measure the SHG output power under different pump powers at 1560 nm (Fig. 3(b)). The frequency conversion efficiency becomes saturated with increased input power. When the on-chip pump power is >1 mW, the conversion efficiency is as high as ~50%, corresponding to a normalized efficiency of 137,000%/W. With the increased CW power, the photorefractive effect [24] becomes severe.

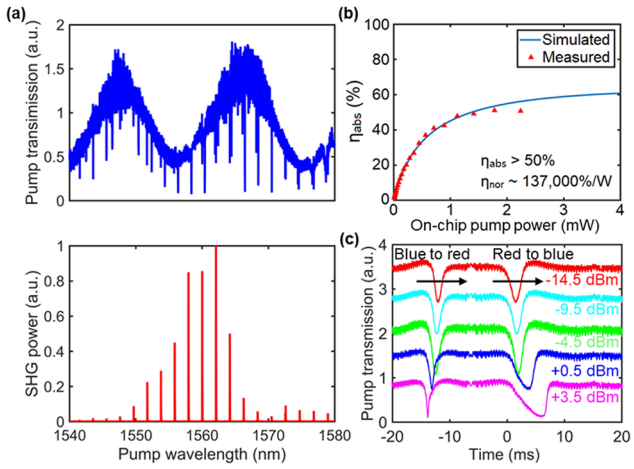

Fig. 3. Transmissions with CW pump frequency scanning. (a) Transmission spectra at pump power of −15 dBm and SHG spectra at pump power of −3 dBm; (b) SHG conversion efficiency at different on-chip pump powers; (c) pump transmissions with different on-chip pump powers. a. u., arbitrary units.

As shown in Fig. 3(c) when the pump laser is scanned from the red to the blue side at 3.5 dBm, the transmission curve exhibits a triangle shape, which means the photorefractive effect is dominant over the thermal effect [24,25]. We attribute the photorefractive effect to the space-charge field due to the oxide-cladding by plasma enhanced chemical vapor deposition (PECVD) [24].

Comb generation with cavity-enhanced SHG. We try to load high CW pump power at 1560 nm to excite the comb generation. However, with more power loaded into the cavity, the photorefraction dominating the thermal effect causes the blueshift of the mode resonances as well as the shift of the phase matching condition by more than several FSRs away from the initial pump wavelength optimized at low power. The imperfect phase matching at high pump power leads to the quench of the resonant SH signal thus the dropped intracavity power. The power dropping then causes the redshift of the resonances thus the effective laser scanning toward the blue side, resulting in the pump laser getting kicked out from the resonance. Therefore, it is difficult to maintain the CW pump in the cavity with the high average power inducing a strong photorefractive effect [24]. In order to alleviate the effect, we switched to the pulsed laser (repetition rate of 1 MHz and pulse duration of 10 ns) with high (on-chip) peak power of 28.2 mW and low average power of 282 μW. We manually tune the pump laser wavelength toward the red side and fix the wavelength when the average output power for the visible band is maximized. With a pulsed pump laser, output spectra are not stable. Therefore, we record the output spectra with maximum intensities (at a maximum hold mode) during a 5-min measurement. Thanks to the high peak power, cascaded quadratic processes, including sum frequency generation (SFG), difference frequency generation (DFG), optical parametric generation (OPG), and SHG, are excited for the comb generation at both bands [Fig. 4(a)]. As shown in Fig. 4(b), the comb bandwidths are 150 and 25 nm for 1560 and 780 nm, respectively.

Comb generation in doubly resonant OPO. To implement frequency comb generation in a doubly resonant OPO (both visible and near-infrared bands are resonant), we also utilize a pulsed

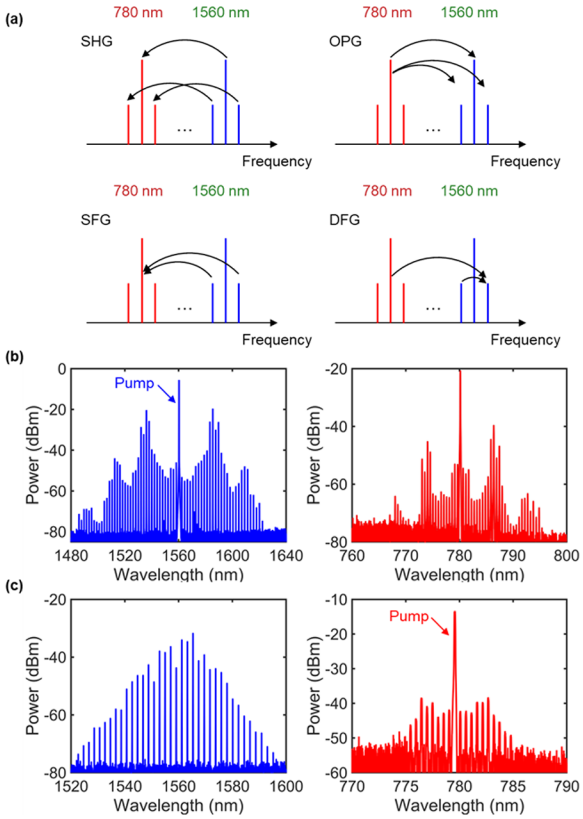

Fig. 4. Comb generation from cascaded quadratic processes. (a) Schematic for the four quadratic processes. Comb generation at the visible band comes from the SHG and SFG processes of the near-infrared combs. Reversely, combs at the visible band also contribute to the combs at the near-infrared band through OPG and DFG processes. (b) Spectra at both bands for the case of cavity-enhanced SHG. (c) Spectra at both bands for the case of OPO. Left: near-infrared band; right: visible band.

visible light (repetition rate of 1 MHz and pulse duration of 10 ns) with high (on-chip) peak power of 4.6 mW and low average power of 46 μW as the pump to trigger cascaded quadratic nonlinear processes. By manually adjusting the pump wavelength and loading the pulsed laser into the cavity from the blue side, we obtain comb generation with maximum intensities (at a maximum hold mode). Comb bandwidths of 80 and 12 nm for 1560 and 780 nm are achieved, respectively, as shown in Fig. 4(c). In Supplement 1, we provide numerical simulations for the cascaded quadratic process-induced comb generation, which agree with the simulation results in Fig. 4. According to the theory, the GVM should be reduced further to support soliton generation. At the next stage, we will alleviate the photorefractive effect by redesigning MgO-doped LN [26,27] microresonators with air cladding to achieve GVM < 10 fs/mm so that a continuous-wave pumped quadratic soliton can be generated [7].

In conclusion, we have demonstrated broadband frequency comb generation through dedicated dispersion engineering in a thin-film LN microresonator. Bandwidths of 150 nm (80 nm) and 25 nm (12 nm) for center wavelengths at 1560 and 780 nm are achieved, respectively, in a cavity-enhanced second-harmonic generation (doubly resonant optical parametric oscillator). Our demonstration paves the way for pure quadratic soliton generation, which is a great complement to dissipative Kerr soliton frequency combs for more interesting nonlinear applications.

Funding. National Science Foundation (ECCS 2048202, OMA 2016244); Office of Naval Research (N00014-21-1-2898, N00014-22-1-2224).

Disclosures. The authors declare no conflicts of interest.

Data availability. Data underlying the results presented in this paper are not publicly available at this time but may be obtained from the authors upon reasonable request.

Supplemental document. See Supplement 1 for supporting content.

REFERENCES

1. T. J. Kippenberg, A. L. Gaeta, M. Lipson, *et al.*, Science **361**, eaan8083 (2018).
2. W. Wang, L. Wang, and W. Zhang, Adv. Photonics **2**, 1 (2020).
3. M. Nie, Y. Xie, B. Li, *et al.*, Prog. Quantum Electron. **86**, 100437 (2022).
4. F. Leo, T. Hansson, I. Ricciardi, *et al.*, Phys. Rev. Lett. **116**, 033901 (2016).
5. S. Mosca, M. Parisi, I. Ricciardi, *et al.*, Phys. Rev. Lett. **121**, 093903 (2018).
6. A.W. Bruch, X. Liu, Z. Gong, *et al.*, Nat. Photonics **15**, 21 (2021).
7. M. Nie and S.-W. Huang, Opt. Lett. **45**, 2311 (2020).
8. M. Nie and S.-W. Huang, Phys. Rev. Appl. **13**, 044046 (2020).
9. M. Nie, Y. Xie, and S.-W. Huang, Nanophotonics **10**, 1691 (2021).
10. Z. Gong, A. W. Bruch, F. Yang, *et al.*, Opt. Lett. **47**, 746 (2022).
11. J. Lu, D. N. Puzyrev, V. V. Pankratov, *et al.*, Nat. Commun. **14**, 2798 (2023).
12. J. Szabados, D. N. Puzyrev, Y. Minet, *et al.*, Phys. Rev. Lett. **124**, 203902 (2020).
13. D. Zhu, L. Shao, M. Yu, *et al.*, Adv. Opt. Photonics **13**, 44 (2021).
14. M. Jin, J. Chen, Y. Sua, *et al.*, Opt. Lett. **46**, 1884 (2021).
15. J. Lu, J. B. Surya, X. Liu, *et al.*, Opt. Lett. **44**, 1492 (2019).
16. J.-Y. Chen, Z.-H. Ma, Y. M. Sua, *et al.*, Optica **6**, 1244 (2019).
17. Z. Ma, J.-Y. Chen, Z. Li, *et al.*, Phys. Rev. Lett. **125**, 263602 (2020).
18. Z. Ma, J. Y. Chen, M. Garikapati, *et al.*, Phys. Rev. Appl. **20**, 044033 (2023).
19. J.-Y. Chen, C. Tang, M. Jin, *et al.*, Laser Photonics Rev. **15**, 2100091 (2021).
20. P.-K. Chen, I. Briggs, C. Cui, *et al.*, Nat. Nanotechnol. **19**, 44 (2023).
21. S.-W. Huang, H. Zhou, J. Yang, *et al.*, Phys. Rev. Lett. **114**, 053901 (2015).
22. M. Nie, K. Jia, Y. Xie, *et al.*, Nat. Commun. **13**, 6395 (2022).
23. Y. Liu, Y. Xuan, X. Xue, *et al.*, Optica **1**, 137 (2014).
24. Y. Xu, M. Shen, J. Lu, *et al.*, Opt. Express **29**, 5497 (2021).
25. J.-Y. Chen, C. Tang, Z.-H. Ma, *et al.*, Opt. Lett. **45**, 3789 (2020).
26. D. A. Bryan, R. R. Rice, R. Gerson, *et al.*, Opt. Eng. **24**, 138 (1985).
27. A. Winnacker, R. M. Macfarlane, Y. Furukawa, *et al.*, Appl. Opt. **41**, 4891 (2002).